Front. Phys. 11(6), 115205 (2016)
DOI 10.1007/s11467-016-0591-4

RESEARCH ARTICLE

Characterization of the globular oxide inclusion ratings in steel using laser-induced breakdown spectroscopy

Yong Zhang[1], Yun-Hai Jia[2,†], Chun Yang[2], Dong-Ling Li[2], Jia Liu[3], Yong-Yan Chen[3], Ying Liu[4], Yi-Xiang Duan[1]

[1] *Research Center of Analytical Instrumentation, Key Laboratory of Bio-Resource and Eco-Environment, Ministry of Education, College of Life Science, Sichuan University, Chengdu 610064, China*
[2] *Central Iron and Steel Research Institute, Beijing 100081, China*
[3] *NCS Testing Technology Co., Ltd., Beijing 100094, China*
[4] *General Research Institute of Nonferrous Metals, Beijing 100088, China*
Corresponding author. E-mail: †jiayunhai@ncschina.com
Received August 18, 2015; accepted March 13, 2016

Grade assessment of steel is generally performed via the metallographic method, which is time-consuming and is not able to provide the elemental distribution information. In this paper, we present a method to measure the globular oxide inclusion ratings in steel using laser-induced breakdown spectroscopy (LIBS). The measurement is performed in two basic steps: steel samples are polished using metallographic sand paper and the Al_2O_3 inclusion number and size distribution in a marked area are observed using scanning electron microscope/energy dispersive X-ray spectroscopy (SEM/EDS) for further LIBS scanning analysis. The threshold intensity that distinguishes soluble aluminum and insoluble aluminum inclusions is determined using LIBS combined with the SEM/EDS statistical data. Carbon steel (the sample number is S9256) and bearing steel (the sample number is GCr15) are analyzed in scanning mode, and the number of Al_2O_3 inclusions in different size ranges is obtained from the statistical information derived from the Al_2O_3 size calibration curve. According to heavy and thin series for globular oxide inclusions grade assessment, the method we propose is comparable to the traditional metallographic method in terms of accuracy; however, the process is simplified and the measurement speed is significantly improved.

Keywords laser-induced breakdown spectroscopy (LIBS), globular oxide inclusion, steel grade assessment, elemental distribution

PACS numbers 52.25.Kn, 52.25.Os

1 Introduction

Nonmetal inclusions in steel have an important influence on the quality of steel. They can decrease the performance of steel in various applications, such as the fatigue property of bearing and heavy railway steel, coating property of car thin plate, and cutting property due to nonmetal inclusions on material surfaces. In addition, nonmetal inclusions influence the quality of steel grades for the production of spring steel, thin sheets and wires. Generally, grade assessment of nonmetal inclusions is performed according to the "steel — determination of content of nonmetallic inclusions — micrographic method using standard diagrams" standard (GB/T 10561-2005/ISO 4967: 1998(E)). However, this method is time-consuming and cannot intuitively provide elemental distribution.

Laser-induced breakdown spectroscopy (LIBS) is a plasma emission spectroscopy tool that has been being developed rapidly in recent years. LIBS is widely used in metallurgical [1–3], geological [4, 5], nuclear [6, 7], and biological industries [8, 9]. The LIBS technique has been extensively reviewed in many aspects, including its fundamentals, instrumentation, and applications [10–14]. LIBS can perform the bulk analysis of various types of samples [15, 16] and can provide the elemental distribution information, which is useful for evaluating material properties.

Bigne [17] proposed a calibration approach to enable

the quantification of the elemental composition of nonmetallic inclusions; the same data were also used to estimate the size of the inclusions. The quantified chemical composition data on nonmetallic inclusions obtained using LIBS were compared to the corresponding results obtained from the scanning electron microscope/energy dispersive X-ray spectroscopy (SEM/EDS) analysis, a conventional method used for steel cleanness assessment, and were proved accurate. Kuss [18] estimated the content of nonmetallic inclusions in ferrous materials using LIBS; signals of inclusion-related elements were evaluated using different statistical algorithms to distinguish the threshold intensity, at which laser pulses focused on the nonmetallic inclusions and the elements dissolved in the metallic matrix. LIBS scanning measurements were performed using samples displaying segregation and decarburization by Bigne [19]. A sample size of 60 × 60 mm^2 with a step size of 50 μm was used, and the resulting quantified elemental maps correlated well with the data from conventional methods. Mateo [20] performed an automated line imaging arrangement for 2D and 3D generation of chemical maps of inclusions in stainless steel using LIBS. In comparison with the point-to-point LIBS mapping method, a 51-fold reduction in the number of pulses and analysis time was achieved when the microline imaging approach was employed. An engine valve composed of different alloys was analyzed using LIBS to prove the capability of this technique to characterize mechanical parts that are complex in terms of shape and composition by Quintas [21]; 3D chemical maps were plotted using a computer application for Fe, Mn, Cr, and Ni elements. These works demonstrate the potential of this technique as an evaluation tool for quality control. Chemical mapping with a lateral resolution of approximately 10 μm of the distribution of precipitates on the surface of aluminum alloys of a sample was performed using LIBS [22]. Two main types of precipitates, Mn–Fe–Cu (type I) and Mg–Cu (type II), were unambiguously distinguished consistently with the X-ray microanalysis measurements.

In this paper, a size calibration curve of nonmetal inclusions, which is used to estimate the size of the inclusions, was constructed using the average size, in contrast to Bigne's method [17], in which a few Al_2O_3 inclusions are selected to establish it. In addition, the inclusion size distribution information acquired from SEM/EDS was used to determine the threshold intensity distinguishing insoluble and soluble aluminum, which is different from Kuss's method [18]. Finally, on the basis of a statistical mathematical model, the globular oxide inclusion ratings of carbon steel and bearing steel were assessed in detail.

2 Experimental setup and parameters

The experimental setup consisted of a Q-switch Nd:YAG laser, sample chamber that could be filled with argon, Paschen–Runge spectrometer, pulse delay generator, and stepper motor, which could drive the sample along the x- and y-axes, as shown in Fig. 1.

The Q-switch Nd:YAG laser (Continuum Surelite III) has an output wavelength of 1064 nm, pulse width of 5.3 ns, pulse energy of 200 mJ, beam waist of approximately 9 mm, focal length of 100 mm, and aperture attenuating energy of 4 mm. The optical path configuration of the spectrometer is Paschen–Runge, and the diameter of the Rowland circle is 750 mm. The grooves of a con-

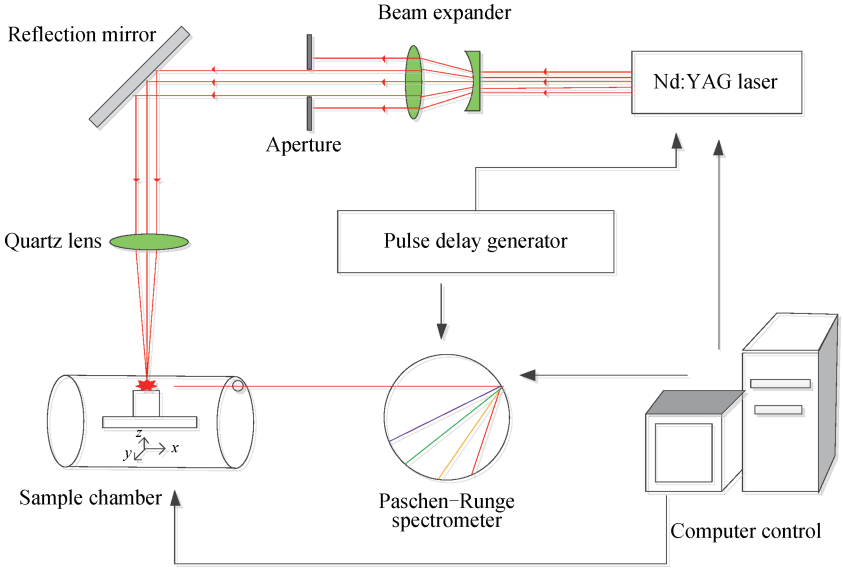

Fig. 1 LIBS experimental setup.

cave grating are 2400 lines/mm, and the resolution of the spectrometer is better than 0.01 nm. The light signal was detected by a photomultiplier tube (PMT), which was installed on the experimental setup, including C, P, and S channels with the resonance line located in the VUV region. A three-axis stepper motor was placed in the sample chamber. The LIBS microanalysis was performed using the stepper motor moving along the x and y directions. The sample chamber was filled with argon, and the pressure was maintained at 7500 Pa. Al I 396.15 nm was used as the analytical line.

Carbon steel (the sample number is S9256) and bearing steel (the sample number is GCr15) were polished using metallographic sand paper, and the statistical distribution of the size of Al_2O_3 inclusions in a marked area was observed using SEM/EDS (JSM 6400, JEOL Ltd, Japan). Al_2O_3 was found to be the main form of nonmetal inclusions in these two types of steel samples. The morphology of laser ablation craters was observed using a metallurgical microscope (Zeizz Vert.A1, Germany). The ablation depth was measured using a 3D optical profilometer (Contour GT, Bruker, Germany).

3 Results and discussion

3.1 Characterization of the globular Al_2O_3 inclusion size using SEM/EDS

The main existing form of nonmetal inclusion was globular Al_2O_3 inclusions in the steel matrix for sample S9256. The shape of the sample was cylindrical, and the sample was cut into four pieces; each piece was polished using the metallographic sample preparation. Five marked areas with equal size were made using LIBS with an area of 3×3 mm^2. The Al_2O_3 size distribution in the five marked areas was determined using SEM/EDS before performing the LIBS scanning analysis. The Al_2O_3 inclusion size distribution in the five marked areas is shown in Table 1.

3.2 Laser ablation morphology

The scanning analysis was performed in the marked areas using LIBS after the Al_2O_3 inclusion size distribution was determined using SEM/EDS. The LIBS measurements were conducted in an argon environment at 7500 Pa in the chamber. The pulse energy and aperture were 200 mJ and 4 mm, respectively, and the step distance was 150 μm along the X and Y directions. The morphology of the laser ablation craters observed using the metallurgical microscope is shown in Fig. 2.

The diameter of the laser ablation craters was approximately 82 μm, and thus the area of the ablation morphology was 0.005 279 mm^2. The scanning area was 3×3 mm^2, and the step distance was 100 μm along the x and y directions, so there were 921 ablation craters. The ratio of the ablation area to the total observed area was approximately 57%. The depth of the ablation craters was approximately 0.5 μm, which was measured using confocal laser scanning microscopy.

3.3 Globular oxide inclusion grade assessment in steel using LIBS

The data acquired using LIBS were organized in descending order. 1445 Al_2O_3 inclusions were totally observed using SEM/EDS in the five marked areas, so the number of the abnormal intensity was $1445 \times 0.57 = 823$. The 823rd data point can be treated as the threshold intensity to distinguish insoluble and soluble aluminum in steel. Based on the Al_2O_3 relative inclusion size distribution, there were 482 abnormal ($823 \times 0.586 = 482$) data points, which corresponded to the threshold intensity at an Al_2O_3 inclusion size of 1 μm, and 302 abnormal data points that corresponded to the intensity produced

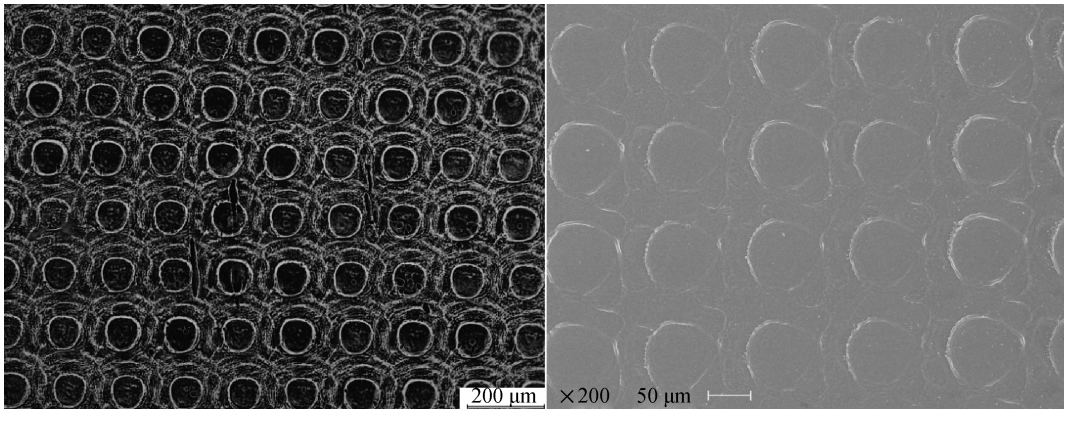

Fig. 2 Morphology of the laser ablation craters observed using the metallographic microscope (left) and the SEM (right).

Table 1 Size distribution of Al_2O_3 inclusions of the five marked areas for carbon steel (the sample number is S9256).

No. scanning area	< 1 μm	1–3 μm	3–5 μm	5–7 μm	7–9 μm	9–11 μm
Region 1#	190	120	16	6	2	1
Region 2#	156	95	6	0	0	0
Region 3#	178	114	10	4	2	1
Region 4#	138	82	14	0	0	0
Region 5#	184	118	8	0	0	0
Total inclusion numbers	846	529	54	10	4	2
Relative distribution of the inclusion size (%)	58.5	36.7	3.7	0.7	0.3	0.1

by an inclusion size in the range of 1–3 μm. Similarly, the number of the abnormal data points associated with other inclusion sizes was obtained. Once the numbers of abnormal data were obtained in different size ranges, they were averaged, and the size calibration curve was constructed by setting the inclusion size as the x-axis and the corresponding intensity as the y-axis. The Al_2O_3 inclusion size calibration curve is shown in Fig. 3.

Employing another cutting quarter sample, a region of 6 × 6 mm^2 was marked using LIBS. Assessment of the steel cleanness grade was conducted according to the "steel — determination of content of nonmetallic inclusions — micrographic method using standard diagrams" national standard. According to the national standard, a heavy series is defined as inclusion diameters in the range of 8–13 μm, and a thin series is defined as inclusion diameters in the range of 3–8 μm. For both series, if the inclusion number amounts are 1–4 and 5–9, the grades are 0.5 and 1.0, respectively. The result of the metallographic grade assessment is that the heavy series is 0.5 and the thin series is 1.0. In consistency with the established size calibration curve experimental conditions, a scanning area of 6 × 6 mm^2 was performed using LIBS, and the step distance was 100 μm along the x and y directions, acquiring 3721 data points in total. The pulse sequence and the 2D elemental distribution map for aluminum are shown in Fig. 4.

As shown in Fig. 4(a), the spectral line intensity for Al I 396.15 nm at some positions was abnormally high, corresponding to a laser pulse hitting insoluble aluminum inclusions. Conversely, relatively low intensities indicate that a laser pulse hit soluble aluminum. From the number of the abnormal intensity locations, the Al_2O_3 inclusion numbers can be obtained. The Al_2O_3 inclusion size can also be obtained from the abnormal intensity. The 2D elemental distribution map for aluminum is shown in Fig. 4b, and different color zones stand for different intensities. From the 2D map of aluminum, the Al_2O_3 inclusion distribution in steel can be obtained.

The observation field of the metallographic inclusion rating was 0.5 mm^2, which corresponded to an area of 0.71 × 0.71 mm^2. The step distance of the stepping motor was 100 μm along the x and y directions, so the

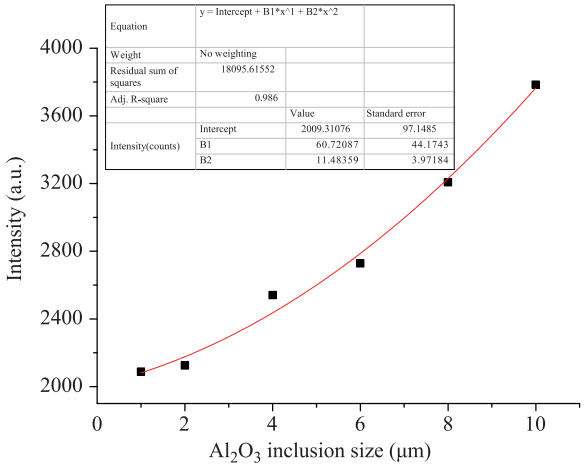

Fig. 3 Al_2O_3 inclusion size calibration curve for sample S9256.

observation field of the metallographic inclusion rating corresponded to 7 × 7 laser ablation craters. The 3721 data points can be changed into a 61 × 61 data matrix, taking a 7 × 7 data matrix as a sliding window. The scanning area and the sliding window are shown in Fig. 5.

Figure 5(a) represents the scanning area, in which the dotted area is enlarged and displayed in Fig. 5(b) as the sliding window. Starting from the first row and the first column, the worst fields were searched in the size ranges of 8–13 μm and 3–8 μm, in which the inclusion numbers were largest. Based on the largest numbers of Al_2O_3 inclusions in the size range of 8–13 μm, the heavy series was evaluated. The thin series was assessed based on the largest numbers of Al_2O_3 inclusions in the size range of 3–8 μm. The acquired data were transformed into a 61 × 61 data matrix. There were three Al_2O_3inclusions, for which the inclusion size was between 8 and 13 μm. The grade of the heavy series was 0.5. There were seven Al_2O_3 inclusions with inclusion sizes between 3 and 8 μm. The grade of the thin series was 1.0, which agreed well with the results of the metallographic grade assessment.

The pretreatment of GCr15 bearing steel was the same as that of S9256 sample. Five areas were marked using

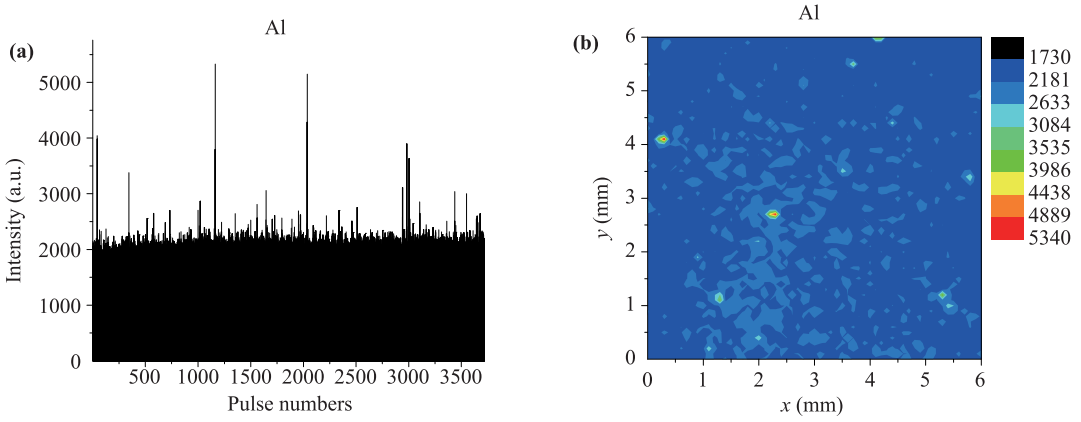

Fig. 4 Pulse sequence and the 2D elemental distribution map for aluminum (the sample number is S9256).

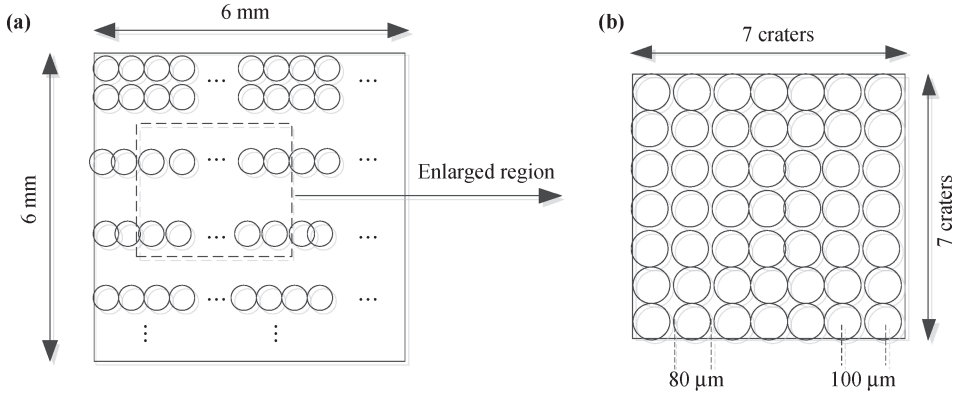

Fig. 5 Schematic diagram of the scanning area and sliding window.

LIBS, with each marked area being 3×3 mm^2. The scanning analysis was performed using LIBS in the marked areas after the Al_2O_3 inclusion size distribution was determined using SEM/EDS, and the data acquired using LIBS were organized in descending order. An Al_2O_3 inclusion size calibration curve was established according to the statistical results obtained using SEM/EDS, and the data treatment was similar to that for S9256 sample. The Al_2O_3 inclusion size calibration curve is shown in Fig. 6.

Another GCr15 bearing sample was polished using metallographic sand paper, on which an area of 5×5 mm^2 was marked using LIBS. The evaluation of the steel cleanness grade was performed using the metallographic microscope method, which showed that the metallographic inclusion rating was 0.5 (three Al_2O_3 inclusions in the size range of 8–13 μm were observed under a magnification of 100) for the heavy series, whereas the thin series was 1.0 (seven Al_2O_3 inclusions in the size range of 3–8 μm were observed under a magnification of 100). The scanning analysis was performed in the area marked using LIBS, and the number of the acquired data points was 2601. The 2601 data points were converted

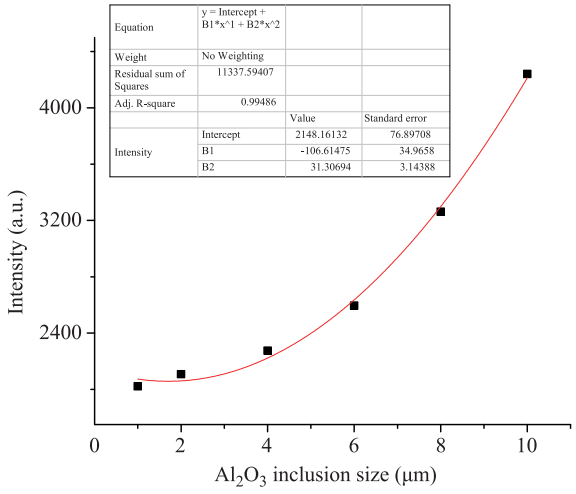

Fig. 6 Al_2O_3 inclusion size calibration curve for GCr15 bearing steel.

into a 51×51 data matrix, from which a 7×7 data matrix was taken as a sliding window. There were three Al_2O_3 inclusions with an inclusion sizes between 8 and 13 μm in the sliding window, and the heavy series grade

Table 2 Comparison of the inclusion rating results for samples S9254 and GCr15 obtained using LIBS and the metallographic method.

	LIBS	metallographic method
Largest number of Al_2O_3 inclusions (sample S9254)	3 (for heavy series) 7 (for thin series)	3 (for heavy series) 6 (for thin series)
Largest number of Al_2O_3 inclusions (sample GCr15)	3 (for heavy series) 8 (for thin series)	3 (for heavy series) 7 (for thin series)
Heavy series (sample S9254)	0.5	0.5
Heavy series (sample GCr15)	0.5	0.5
Thin series (sample S9254)	1	1
Thin series (sample GCr15)	1	1

was 0.5. There were eight Al_2O_3 inclusions with inclusion sizes between 3 and 8 μm in the sliding window, indicating a grade of the thin series of 1.0. The results of the grade assessment agreed with those obtained employing the metallographic method. The results of the grade assessment of samples S9254 and GCr15 obtained using LIBS and the metallographic method are compared in Table 2.

4 Conclusion

Traditionally, the globular oxide inclusion ratings in steel are evaluated via the metallographic method; however, this method is time-consuming, requiring a few hours to evaluate the steel cleanness grade. In this study, the globular oxide inclusion ratings of carbon steel (sample S9256) and bearing steel (GCr15) samples were evaluated using the LIBS scanning mode, and the Al_2O_3 inclusion size distribution was obtained using SEM/EDS. The intensities of insoluble and soluble aluminum hit by a laser pulse could be distinguished based on a mathematical model, and an Al_2O_3 inclusion size calibration curve was established. The results of the metallographic inclusion rating obtained using LIBS agreed well with those obtained utilizing the metallographic microscope method, and LIBS only required approximately 25 min to acquire 961 data points. Therefore, the LIBS method can be used to rapidly evaluate the globular oxide inclusion rating in steel.

Acknowledgements This work was supported by the National Key Scientific Instrument and Equipment Development Project, China (Grant No. 2012YQ20018208).

References

1. R. Noll, C. F. Begemann, M. Brunk, S. Connemann, C. Meinhardt, M. Scharun, V. Sturm, J. Makowe, and C. Gehlen, Laser-induced breakdown spectroscopy expands into industrial applications, *Spectrochim. Acta B* 93, 41 (2014)
2. V. Sturm, J. Vrenegor, R. Noll, and M. Hemmerlin, Bulk analysis of steel samples with surface scale layers by enhanced laser ablation and LIBS analysis of C, P, S, Al, Cr, Cu, Mn and Mo, *J. Anal. At. Spectrom.* 19(4), 451 (2004)
3. A. Sarkar, V. Karki, S. K. Aggarwal, G. SMaurya, R. Kumar, A. K. Rai, X. Mao, and R. E. Russo, *Spectrochim. Acta B* 108, 8 (2015)
4. R. S. Harmon, R. E. Russo, and R. R. Hark, Applications of laser-induced breakdown spectroscopy for geochemical and environmental analysis: A comprehensive review, *Spectrochim. Acta B* 87, 11 (2013)
5. R. Harmon, K. Shughrue, J. Remus, M. Wise, L. East, and R. Hark, Can the provenance of the conflict minerals columbite and tantalite be ascertained by laser-induced breakdown spectroscopy? *Anal. Bioanal. Chem.* 400(10), 3377 (2011)
6. M. Z. Martin, S. Allman, D. J. Brice, R. CMartin, and N. O. Andre, Exploring laser-induced breakdown spectroscopy for nuclear materials analysis and *in-situ* applications, *Spectrochim. Acta B* 74–75, 177 (2012)
7. D. A. Cremers, A. Beddingfield, R. Smithwick, R. C. Chinni, C. R. Jones, B. Beardsley, and L. Karch, Monitoring uranium, hydrogen, and lithium and their isotopes using a compact laser-induced breakdown spectroscopy (LIBS) probe and high-resolution spectrometer, *Appl. Spectrosc.* 66(3), 250 (2012)
8. M. Galiová, J. Kaiser, K. Novotný, J. Novotný, T. Vaculovi? M. Liška, R. Malina, K. Stejskal, V. Adam, and R. Kizek, Investigation of heavy-metal accumulation in selected plant samples using laser induced breakdown spectroscopy and laser ablation inductively coupled plasma mass spectrometry, *Appl. Phys. A* 93(4), 917 (2008)
9. F. M. V. Pereira, D. M. B. P. Milori, A. L. Venâncio, M. S. T. Russo, P. K. Martins, and J. F. Astúa, Evaluation of the effects of Candidatus Liberibacter asiaticus on inoculated citrus plants using laser-induced breakdown spectroscopy (LIBS) and chemometrics tools, *Talanta* 83(2), 351 (2010)
10. J. D. Winefordner, I. B. Gornushkin, T. Correll, E. Gibb, B. W. Smith, and N. Omenetto, Comparing several atomic spectrometric methods to the super stars: special emphasis on laser induced breakdown spectrometry, LIBS, a future super star, *J. Anal. At. Spectrom.* 19(9), 1061 (2004)
11. Z. Wang, T. B. Yuan, Z. Y. Hou, W. D. Zhou, J. D. Lu, H. B. Ding, and X. Y. Zeng, Laser-induced breakdown spectroscopy in China, *Front. Phys.* 9(4), 419 (2014)
12. J. Yu and R. E. Zheng, Laser-induced plasma and laser-induced breakdown spectroscopy (LIBS) in China: The challenge and the opportunity, *Front. Phys.* 7(6), 647 (2012)
13. D. W. Hahn and N. Omennetto, Laser-Induced Breakdown Spectroscopy (LIBS), Part II: Review of instrumental and methodological approaches to material analysis and applications to different fields, *Appl. Spectrosc.* 66(4), 347 (2012)

14. G. Cristoforetti, E. Tognoni, and L. A. Gizzi, Thermodynamic equilibrium states in laser-induced plasmas: From the general case to laser-induced breakdown spectroscopy plasmas, *Spectrochim. Acta B* 90, 1 (2013)

15. J. Kaiser, M. Galiová, K. Novotný, R. Červenka, L. Reale, J. Novotný, M. Liška, O. Samek, V. Kanický, A. Hrdlička, K. Stejskal, V. Adam, and R. Kizek, Mapping of lead, magnesium and copper accumulation in plant tissues by laser-induced breakdown spectroscopy and laser-ablation inductively coupled plasma mass spectrometry, *Spectrochim. Acta B* 64(1), 67 (2009)

16. V. Motto-Ros, L. Sancey, X. C. Wang, Q. L. Ma, F. Lux, X. S. Bai, G. Panczer, O. Tillement, and J. Yu, Mapping nanoparticles injected into a biological tissue using laser-induced breakdown spectroscopy, *Spectrochim. Acta B* 87, 168 (2013)

17. F. Boué-Bigne, Analysis of oxide inclusions in steel by fast laser-induced breakdown spectroscopy scanning: An approach to quantification, *Appl. Spectrosc.* 61(3), 333 (2007)

18. H. M. Kuss, H. Mittelstaedt, and G. Mueller, Inclusion mapping and estimation of inclusion contents in ferrous materials by fast scanning laser-induced optical emission spectrometry, *J. Anal. At. Spectrom.* 20(8), 730 (2005)

19. F. Boué-Bigne, Simultaneous characterization of elemental segregation and cementite networks in high carbon steel products by spatially-resolved laser-induced breakdown spectroscopy, *Spectrochim. Acta B* 96, 21 (2014)

20. M. P. Mateo, L. M. Cabalin, J. M. Baena, and J. J. Laserna, Surface interaction and chemical imaging in plasma spectrometry induced with a line-focused laser beam, *Spectrochim. Acta B* 57(3), 601 (2002)

21. I. Lopez-Quintas, M. P. Mateo, V. Piñon, A. Yañez, and G. Nicolas, Mapping of mechanical specimens by laser induced breakdown spectroscopy method: Application to an engine valve, *Spectrochim. Acta B* 74–75, 109 (2012)

22. I. V. Cravetchi, M. Taschuk, Y. Y. Tsui, and R. Fedosejevs, Scanning microanalysis of Al alloys by laser-induced breakdown spectroscopy, *Spectrochim. Acta B* 59(9), 1439 (2004)